Journal of Physics D: Applied Physics

PAPER

Topologically protected energy-time entangled biphoton states in photonic crystals

To cite this article: Zhen Jiang *et al* 2022 *J. Phys. D: Appl. Phys.* **55** 315104

IOP Publishing Journal of Physics D: Applied Physics

J. Phys. D: Appl. Phys. **55** (2022) 315104 (8pp) https://doi.org/10.1088/1361-6463/ac6f2d

Topologically protected energy-time entangled biphoton states in photonic crystals

Zhen Jiang, Chaoxiang Xi, Guangqiang He* and Chun Jiang*

State Key Laboratory of Advanced Optical Communication Systems and Networks, Shanghai Jiao Tong University, Shanghai 200240, People's Republic of China

E-mail: gqhe@sjtu.edu.cn and cjiang@sjtu.edu.cn

Received 14 March 2022, revised 30 April 2022
Accepted for publication 12 May 2022
Published 23 May 2022

Abstract

The concepts of topological phases have been widely exploited in quantum optics in recent years. Here we demonstrate a topological insulator implementing topological protection of correlated biphoton states. A degenerate four-wave mixing (FWM) process of pseudospin states propagating along the topological interface is numerically simulated. Strikingly, the signal and idler photons generated from the FWM process are clarified to be entangled between two degrees of freedom—the frequencies of photon pairs and their time of arrival. The topological edge states of the pump, signal, and idler are robust against the sharp bends and defects, revealing the topological protection of energy-time entangled biphoton states. These findings could pave the way for unprecedented topological quantum devices.

Keywords: topological insulators, entangled biphoton states, energy-time entanglement

(Some figures may appear in colour only in the online journal)

1. Introduction

Topological insulators, promising platforms possessing insulating bulk and topological edge states, have become a rapidly burgeoning field in condensed matter physics. Promptly, photonic analogs of topological insulators have been manipulated in different topological models including the quantum Hall effect [1, 2], quantum spin Hall (QSH) effect [3–5], quantum valley Hall (QVH) effect [6–8], and high-order topological systems [9–11]. Topological photonic systems [12] emulating the QSH effect support topologically protected pseudospin states at the interface between photonic crystals with different topological phases. Topological edge states protected by the crystal symmetry show prominent topological properties, including robustness against sharp bends and structural imperfections.

Most recently, the concepts of topological phases were exploited in nonlinear and quantum optics. Comprehensive approaches to the advances revealing topologically protected second- or third-harmonic generation were implemented in topological metasurfaces [13], second-order topological insulators [14, 15], and silicon nanoparticles [16]. Moreover, a graphene metasurface governing topological edge plasmons with nonlinear spontaneous four-wave mixing (FWM) process has been demonstrated theoretically [17]. At the same time, the exploitation of topological protection in quantum systems has led to an affecting field, which refers to topological quantum optics. Thus the generation and protection of quantum states have been closely tied to topological photonics, such as topological single quantum emitters [18], topological quantum sources [19, 20], topological biphoton quantum states [21, 22], topological quantum walks of correlated photons [23, 24], topologically protected path-entangled states [25] and topological protection of quantum coherence [26, 27]. These approaches of topological quantum optics show that the topology nature can bring robustness to quantum systems.

* Authors to whom any correspondence should be addressed.

We have shown that topologically protected continuous frequency entangled biphoton states can be manipulated in a QVH system [28]. Here we propose topologically protected energy-time entangled biphoton states in topological photonic crystals emulating the QSH effect. In particular, we study the dispersion relation of photonic crystals and manipulate a degenerate FWM process. The quantum correlation between signal and idler photons generated from the FWM process is clarified. We theoretically proved that the biphoton state is energy-time entangled. The result manifests that the topological edge states of biphotons are robust against the sharp bends and defects, confirming the topological protection of entangled biphoton states. From an underlying perspective, our proposal provides a platform for bringing the concepts of topological photonics to the realm of quantum systems.

2. Topological photonic crystals

Topological photonic systems provide a practical way for exhibiting topological protection of correlated photon pairs generated from the nonlinear spontaneous FWM process. For a degenerate FWM process, two pump photons with the frequency ω_p are annihilated, and a pair of photons, refer as the signal (ω_s) and idler (ω_i), are generated simultaneously. The relations between four photons of the FWM process are described by energy and momentum conservation conditions, $2\hbar\omega_p = \hbar\omega_s + \hbar\omega_i$ and $2k_p = k_s + k_i$, where k_p, k_s and k_i represent the wavevectors of the pump, signal, and idler respectively. Here we study topologically protected entangled biphoton states in silicon-based topological photonic crystals. As shown in figure 1(a), the photonic crystal structure is composed of deformed honeycomb lattices possessing C_6 symmetry. With the excitation of the pump, a nonlinear spontaneous FWM process occurs at the interface between trivial and nontrivial photonic crystals. In particular, the correlated signal and idler photons generated by the FWM process are entangled, giving evidence of the quantum nature of the topological system. Since the frequencies of the pump, signal, and idler are localized inside the operation bandwidth of topological edge states, the entangled signal and idler photons are topologically protected due to the topological nature of the QSH effect.

The 2D close-up image of topological photonic crystals exciting the QSH effect is illustrated in figure 1(b), where R is a radius of the hexagon cluster, r is a radius of each silicon rod, a is regarded as the lattice constant. For an unperturbed honeycomb lattice ($R = a/3$), there appears a fourfold degenerate Dirac cone at the K and K' points in the first Brillouin zone due to the six-fold rotational symmetry of the unit cell [12, 29]. When an unperturbed honeycomb lattice is concentrically compressed to $R = 0.9a/3$ without the breaking of C_6 crystal symmetry, a topological trivial band gap emerges in the vicinity of the Γ point as shown in figure 1(c). Similarly, when an unperturbed honeycomb lattice is concentrically expanded to $R = 1.1a/3$ without the breaking of C_6 crystal symmetry, the band structure is topological nontrivial [12]. The band structure of expanded unit cells is plotted in figure 1(d), the photonic bandgap reopens in the vicinity of the Γ point.

One must take into account that with the transformation from the trivial band structure to the nontrivial case, the bands of dipolar modes (p_x/p_y) and quadrupolar modes ($d_{x^2-y^2}/d_{xy}$) are reversed, referring to band inversion. Moreover, the spin Chern numbers of trivial and nontrivial photonic crystals are identified as $C_s = 0$ and $C_s = \pm 1$ respectively [12]. As is well known, the topologically protected edge states exist at the interface between trivial and nontrivial photonic crystals.

3. Nonlinear FWM process of pseudospin states

The band inversion of eigenmodes provides a prerequisite for the QSH effect, which gives rise to topological edge states. In order to study the underlying properties of topological edge states, we calculate the dispersion relation of topological photonic crystals composed of trivial and nontrivial regions. As shown in figure 2(a), the result reveals that a pair of edge states exist within the topological bandgap. As a result of the QSH effect, the two edge states have opposite chirality, which refers to pseudospin-up (σ^+) states and pseudospin-down (σ^-) states [30, 31]. Specifically, different pseudospins lock to counter-propagating edge states at the topological interface. Interestingly, the dispersion slopes of topological edge states are almost linear, leading to an expedient for designing the FWM process. The edge modes within the topological bandgap are topologically protected by crystal symmetry. A remarkable feature of topology protection is the robustness against disorder and defects [12, 31].

To manipulate topologically protected FWM processes, the frequencies of the pump, signal, and idler should be localized inside the topological bandgap. To implement the nonlinear FWM process in topological photonic crystals, the phase-matching condition should be taken carefully. The energy matching condition ($2\hbar\omega_p = \hbar\omega_s + \hbar\omega_i$) is conserved for the FWM process. Thus, the momentum matching condition has become a crucial element for the generation of FWM processes. It is demonstrated that the conversion efficiency of pump photons is largest with the conservation of the momentum matching condition ($2k_p = k_s + k_i$). To this end, we calculate the wavevector mismatch $\Delta k = 2k_p - k_s - k_i$ according to the dispersion relation of pseudospin states as illustrated in figure 2(b). Here the frequencies of the FWM process are considered as $\upsilon_p = 193.3$ THz, $\upsilon_s = 193.6$ THz, and $\upsilon_i = 193.0$ THz respectively. According to the map, the wavevector mismatch of this FWM process is $\Delta k = 6.20 \times 10^{-7}$. As common wisdom of nonlinear optics, more FWM processes emerge with the small value of wavevector mismatch.

To get insight into the topological behaviors of the FWM process, we numerically simulate the electric field distribution of the FWM process in proposed photonic crystals. Figure 3 shows the simulation of this nonlinear process at a trapezoidal interface between trivial and nontrivial regions. A left-handed circularly polarized source is applied to excite pseudospin down (σ^-) states at the frequencies of the pump and signal,

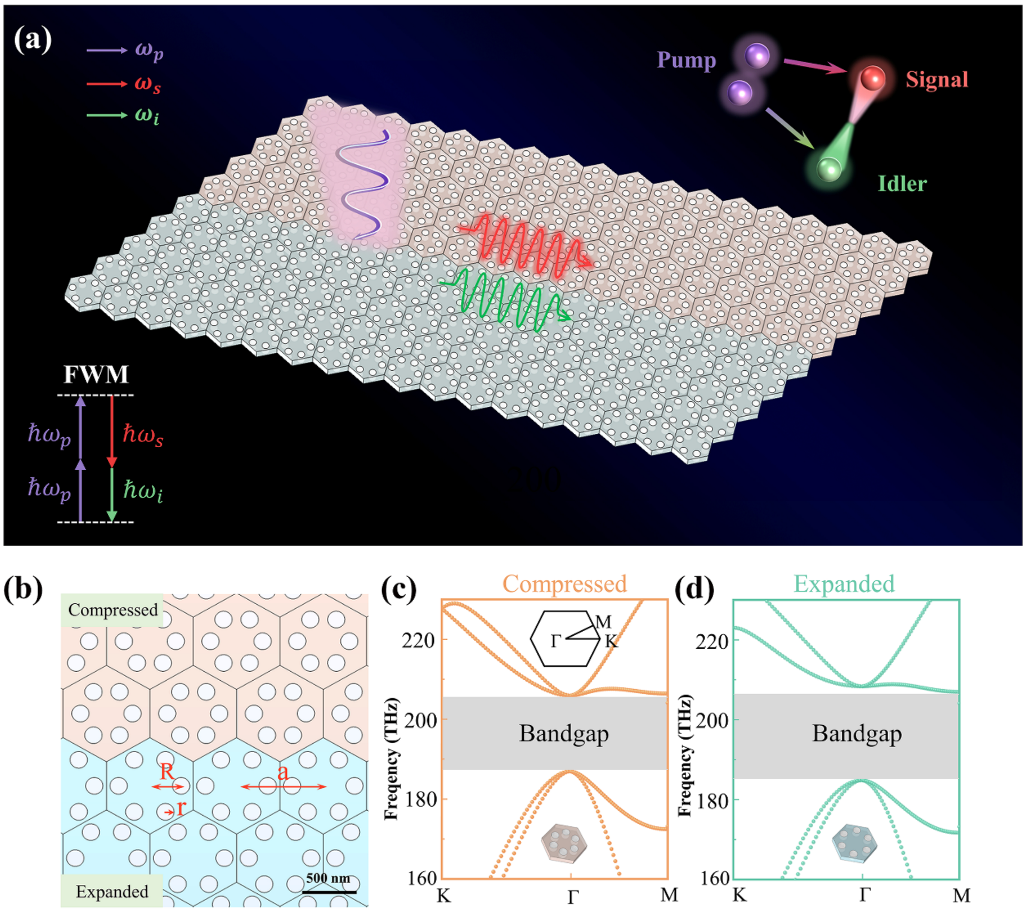

Figure 1. A scheme of the topological photonic system. (a) Schematic of silicon-based photonic crystals exhibiting topological protection of entangled photon pairs, the inset shows a process of degenerate FWM, where two pump photons are annihilated and the signal and idler are generated simultaneously. (b) 2D close-up image of topological photonic crystals exciting QSH effect, with the lattice constant $a = 785$ nm, the radius of each silicon rod $r = 0.11a$. (c) Calculated band structure of trivial photonic crystals ($R = 0.9a/3$). (d) Calculated band structure of nontrivial photonic crystals ($R = 1.1a/3$).

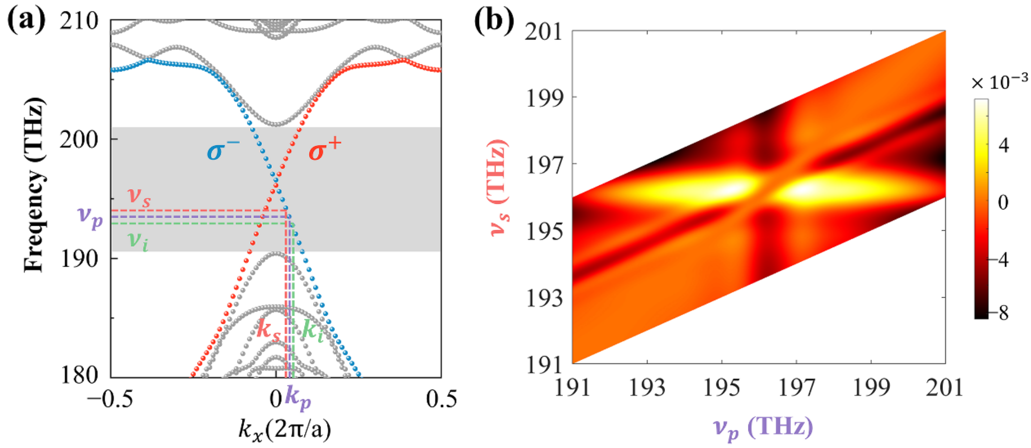

Figure 2. (a) Dispersion relation of topological photonic crystals composed of trivial and nontrivial regions, where σ^+ and σ^- denote pseudospin-up and pseudospin-down states. The frequencies of the FWM process are $\upsilon_p = 193.3$ THz, $\upsilon_s = 193.6$ THz and $\upsilon_i = 193.0$ THz respectively. (b) Map of the calculated wavevector mismatch Δk of topological photonic crystals.

however, there is no input for the idler. By considering the third-order nonlinear susceptibility tensor $\chi^{(3)}$ of silicon, the FWM process is implemented by the coupling of electromagnetic models of the pump, signal, and idler.

As depicted in figures 3(a) and (b), the electric fields of topological edge states at the frequencies of the pump (υ_p) and signal (υ_s) are confined around the topological interface. It is worth mentioning that topological edge states lock to the

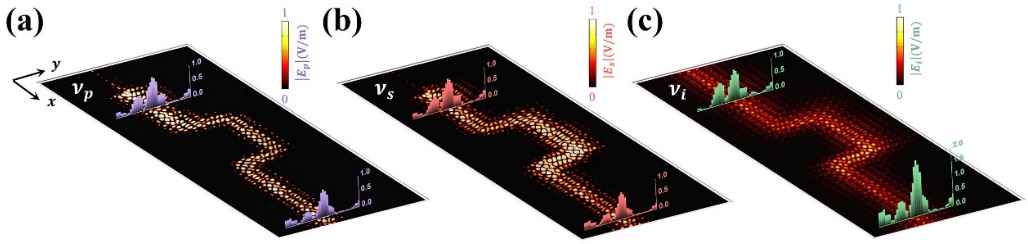

Figure 3. Topologically protected FWM process in proposed photonic crystals. Field profiles of the topological edge states at the frequencies of (a) the pump ($\upsilon_p = 193.3$ THz), (b) signal ($\upsilon_s = 193.6$ THz), and (c) idler ($\upsilon_i = 193.0$ THz) respectively.

pseudospins of the excitation [12], where the pseudospin up locks to backward propagation and the pseudospin down locks to forward propagation. Besides, the propagating direction of topological edge states is also dependent on the position of the excitation [32]. As expected, the one-way propagating edge states can transport through sharp bends without visible backreflection, showing robustness against defects. In addition, two probes are placed around the input and output ports to monitor the energy distributions of edge states. It can be observed that the normalized transmissions of edge states at the frequencies of the pump (υ_p) and signal (υ_s) are nearly unit even part of them are transferred to the idler, which gives clear evidence of the robustness of topological edge states.

As shown in figure 3(c), the edge state at the idler frequency is excited at the topological interface due to the nonlinear FWM process. The edge state of the idler also shows robustness against sharp bends. This provides important validation for the topological nature of the FWM process and further underscores the topological protection of correlated photon pairs generated from the FWM process. Moreover, the normalized transmission implies that the field profile of the idler is amplified along the interface. Notably, we note that the propagating direction of the edge state at the idler frequency is not unidirectional. While the edge states of the pump and signal are excited unidirectionally, for the edge state of the idler, indeed, both pseudospin up and down states are generated. To analyze this, part of the left-handed circularly polarized source is conversed into the right-handed circularly polarization, which refers to circular polarization conversion [13]. The left-handed and right-handed circular polarization leads to forward and backward propagation respectively. One can emphasize that the edge states of the pump, signal, and idler are topologically protected due to the overlap between the topological bandgap and frequencies of FWM interactions. Last but not least, this behavior provides a practical implementation of topological protection of entangled photon pairs generated from the nonlinear FWM interaction.

4. Topological protection of energy-time entanglement

The signal and idler produced via the nonlinear FWM process may lead to entangled states. The continuous frequency entanglement between photon pairs generated via the FWM process in a QVH system has been clarified [28]. Such continuous frequency entanglement describes the frequency correlation between signal and idler photons, revealing that the joint spectral amplitude (JSA) $A(\omega_s,\omega_i)$ cannot be factorized into the function of ω_s and ω_i. Here we discuss the energy-time entanglement between signal and idler photons in a QSH system. Energy-time entanglement is a crucial quantum phenomenon that reveals the correlations between two degrees of freedom—the frequencies of biphotons and their time of arrival. To implement the energy-time entanglement between photon pairs, uncertainty relations [33] must be violated. Generally, two energy-time entangled photons should satisfy the inequality [34]

$$\Delta(\omega_s+\omega_i)\Delta(t_s-t_i) < 1, \tag{1}$$

where ω_s and ω_i are the frequencies of the signal and idler photons, t_s and t_i are the arrival time, $\Delta(\omega_s+\omega_i)$ is the standard deviation of the joint spectrum intensity and $\Delta(t_s-t_i)$ the standard deviation of the joint temporal intensity.

To theoretically evaluate the entanglement between signal and idler photons generated from the FWM process, spectral and temporal measurements should be employed. A pure energy-time biphoton state via the FWM process can written as

$$|\Psi\rangle = \iint \mathrm{d}\omega_s \mathrm{d}\omega_i A(\omega_s,\omega_i)\hat{a}^\dagger_{\omega_s}\hat{a}^\dagger_{\omega_i}|0\rangle, \tag{2}$$

where $A(\omega_s,\omega_i)$ is the JSA. Taking into consideration of the phase-matching condition of the nonlinear FWM process in topological photonic systems, the JSA is approximately modeled by [35]

$$A(\omega_s,\omega_i) = \alpha\left(\frac{\omega_s+\omega_i}{2}\right)\Phi(\omega_s,\omega_i), \tag{3}$$

with the spectrum envelope of the pump takes a form of $\alpha\left(\frac{\omega_s+\omega_i}{2}\right) = \delta(\omega_s+\omega_i-2\omega_p)$. And the joint phase-matching spectrum is given by $\Phi(\omega_s,\omega_i) = \mathrm{sinc}\left(\frac{\Delta kL}{2}\right)$, where the wavevector mismatch is $\Delta k = 2k_p - k_s - k_i$ and L is the propagating length of topological edge states.

The JSA describing the spectral correlations between signal and idler photons generated from the FWM process in topological photonic crystals is depicted in figure 4(a). The result shows strong anticorrelation in the joint spectral intensity. Whereas the joint temporal amplitude (JTA) can be derived by the Fourier transform of JSA [36]

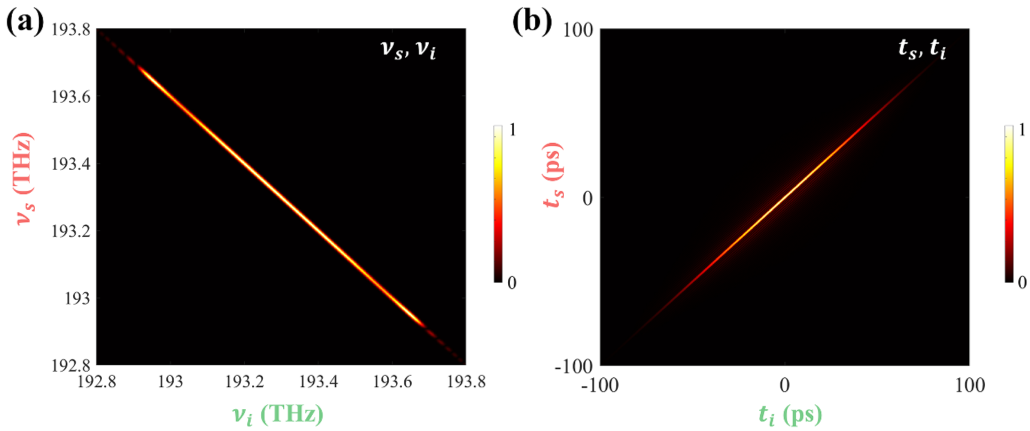

Figure 4. (a) JSA and (b) JTA distributions of biphoton states produced via the FWM process in topological photonic crystals.

$$\widetilde{A}(t_s, t_i) = \iint \mathrm{d}\omega_s \mathrm{d}\omega_i A(\omega_s, \omega_i) \mathrm{e}^{i\omega_s t_s} \mathrm{e}^{i\omega_i t_i}, \tag{4}$$

where the JTA characterizes the temporal correlation between signal and idler photons generated from the FWM process in topological photonic crystals, as shown in figure 4(b). The JTA shows strong positive correlations in joint temporal intensity.

To certify the presence of entanglement [36], we calculate the standard deviation of the joint spectrum intensity $\Delta(\omega_s + \omega_i)$ and joint temporal intensity $\Delta(t_s - t_i)$. According to the JSA and JTA, we decompose the spectral and temporal correlations into the analysis space of $\omega_s + \omega_i$ and $t_s - t_i$. For the biphoton states produced via the FWM process in topological photonic crystals, we calculate the standard deviation as $\Delta(\omega_s + \omega_i) = 3.74 \times 10^9$ Hz and $\Delta(t_s - t_i) = 4.09 \times 10^{-11}$s respectively. Therefore, the joint uncertainty product of the biphoton state is calculated as $\Delta(\omega_s + \omega_i)\Delta(t_s - t_i) = 0.1529$, which satisfies the inequality of equation (1) clarifying the energy-time entanglement. One remarkable conclusion of the theoretical deduction is that topologically protected biphoton states produced via the FWM process are energy-time entangled.

5. Conclusion

In this work, we have demonstrated a topological insulator that implements topological protection of energy-time entangled biphoton states. A degenerate FWM process in proposed topological photonic crystals is numerically simulated. In particular, with the overlap between the topological bandgap and frequencies of the FWM process, the topological edge states of the pump, signal, and idler are robust against sharp bends and structure imperfections, confirming the topological protection of the system. Moreover, we theoretically calculate the JSA and JTA of biphoton states produced via the FWM process. And the energy-time entanglement between signal and idler photons generated from the FWM process is certified. The topological protection of entangled states gives rise to novel on-chip nanophotonic quantum devices.

Data availability statement

The data that support the findings of this study are available upon reasonable request from the authors.

Acknowledgments

This work is supported by the Key-Area Research and Development Program of Guangdong Province (2018B030325002), the National Natural Science Foundation of China (62075129, 61975119).

Conflict of interest

The authors declare that they have no conflict of interest.

Appendix A. Numerical simulation

Finite-element method solver COMSOL Multiphysics is applied to simulate the degenerate FWM process in topological photonic crystals. To perform the nonlinear elements in proposed photonic crystals, the third-order susceptibility tensor of silicon [37] is considered as a constant scalar value of $\chi^{(3)} = 2.45 \times 10^{-19}$ m^2 V^{-2}, with the refractive index of $n_{\mathrm{Si}} = 3.45$. The FWM process is performed by the nonlinear polarizations of silicon

$$\boldsymbol{P}_p(\omega_s + \omega_i - \omega_p) = 6\varepsilon_0\chi^{(3)} E_s E_i E_p^*, \tag{5}$$

$$\boldsymbol{P}_s(\omega_p + \omega_p - \omega_i) = 3\varepsilon_0\chi^{(3)} E_p E_p E_i^*, \tag{6}$$

$$\boldsymbol{P}_i(\omega_p + \omega_p - \omega_s) = 3\varepsilon_0\chi^{(3)} E_p E_p E_s^*, \tag{7}$$

where $\boldsymbol{P}_{p,s,i}$ and $E_{p,s,i}$ denote the polarizations and electric field of the pump, signal, and idler. The FWM process is implemented by the coupling of electromagnetic models of the pump, signal, and idler. A left-handed circularly polarized source is applied to excite pseudospin down (σ^-) states at the frequencies of the pump and signal, however, there is no input for the

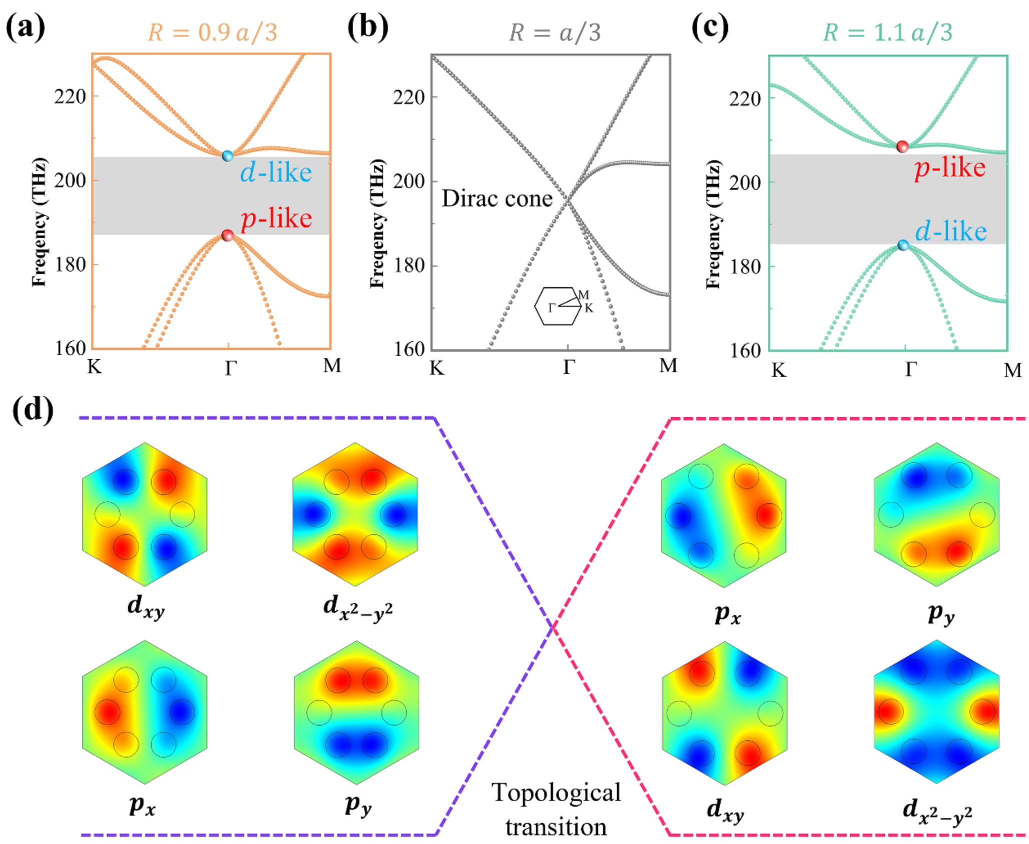

Figure 5. Calculated band structure of (a) trivial ($R = 0.9a/3$), (b) unperturbed ($R = a/3$) and (c) nontrivial unit cells ($R = 1.1a/3$) respectively. (d) Topological band inversion between dipolar modes (p_x/p_y) and quadrupolar modes ($d_{x^2-y^2}/d_{xy}$).

idler. Hence, the generation of field profiles of the idler reveals the emergence of the FWM process.

Appendix B. Spin Chern numbers of honeycomb lattices

By applying the $\vec{k}\cdot\vec{p}$ perturbation theory and tight-binding model, we can obtain the spin Chern number of the deformed honeycomb lattice. For honeycomb lattices with C_6 symmetry, there appear two irreducible representations (E_1 and E_2), which correspond to dipolar and quadrupolar modes. These eigenvalues are given by $\{E_p, E_p, E_d, E_d\} = \{-M-Nk^2, -M-Nk^2, M+Nk^2, M+Nk^2\}$ based on the sets of $(|p_x>, |p_y>, |d_{x^2-y^2}>, |d_{xy}>)$, where $M = (E_d - E_p)/2$. When the unit cell of honeycomb lattices is deformed from the trivial ($R = 0.9a/3$) to nontrivial case ($R = 1.1a/3$), the bands of dipolar modes (p_x/p_y) and quadrupolar modes ($d_{x^2-y^2}/d_{xy}$) are reversed. Figure 5 shows the band structures of the trivial ($R = 0.9a/3$), unperturbed ($R = a/3$) and nontrivial unit cells ($R = 1.1a/3$) respectively. These band structures certify the emergence of the topological bandgap for deformed honeycomb photonic crystals. Moreover, the process of topological band inversion between dipolar modes (p_x/p_y) and quadrupolar modes ($d_{x^2-y^2}/d_{xy}$) is illustrated in figure 5(d). The mechanism of topological transition gives rise to the emergence of topological edge states.

The Hamiltonian describing the band structure of honeycomb lattices can be written as [12]

$$\boldsymbol{H}(k) = \begin{pmatrix} -M+Bk^2 & Ak_+ & 0 & 0 \\ A^*k_- & M-Bk^2 & 0 & 0 \\ 0 & 0 & -M+Bk^2 & Ak_- \\ 0 & 0 & A^*k_+ & M-Bk^2 \end{pmatrix}, \tag{8}$$

with $k_\pm = k_x \pm ik_y$ and $B = -(D+F+2N)/2$. It is noted that this form is similar to the Hamiltonian of Bernevig–Hughes–Zhang model [38]. Moreover, the parameters D, F and A can be calculated by [30]

$$-Dk_x^2 - Fk_y^2 = \frac{\langle p_x|k\cdot P|d_{x^2-y^2}\rangle\langle d_{x^2-y^2}|k\cdot P|p_x\rangle + \langle p_x|k\cdot P|d_{xy}\rangle\langle d_{xy}|k\cdot P|p_x\rangle}{E_p - E_d}, \tag{9}$$

$$Ak_x = \langle p_x|k\cdot P|d_{x^2-y^2}\rangle. \tag{10}$$

The spin Chern number for honeycomb lattices yields [12]

$$C_s = \pm[\mathrm{sgn}(M) + \mathrm{sgn}(B)]/2. \tag{11}$$

Therefore, the spin Chern number is calculated as $C_s = 0$ with $M = (E_d - E_p)/2 > 0$ for the trivial band structure, while $C_s = \pm 1$ with $M = (E_d - E_p)/2 < 0$ for the nontrivial case [12]. It

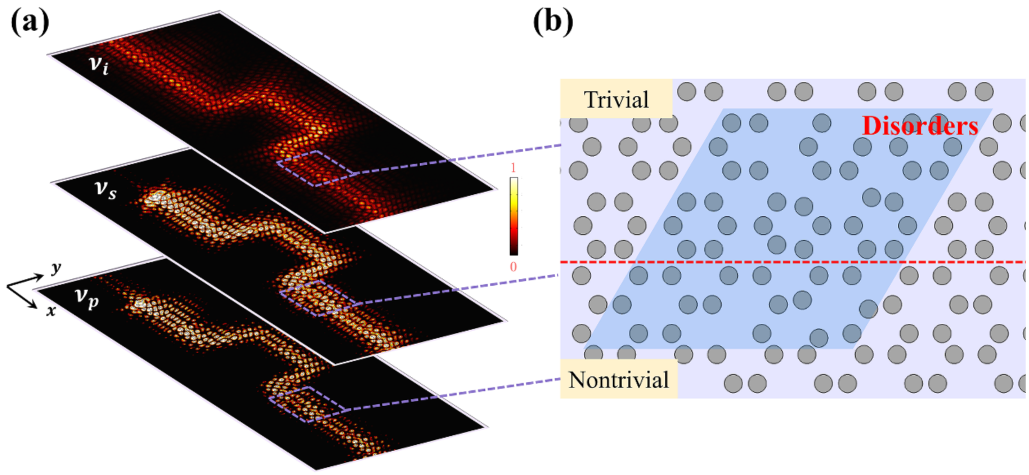

Figure 6. (a) Simulate field profiles of the FWM process in photonic crystals with disorders. (b) Artificial disorders at the interface.

can be proved by the band inversion of p_x/p_y and $d_{x^2-y^2}/d_{xy}$ for the trivial and nontrivial topology.

Appendix C. Nonlinear evolution of the FWM process

Due to the third-order nonlinearity of silicon, the nonlinear FWM process produces the signal and idler photons. For the FWM process, the Hamiltonian is described by

$$H = H_{\rm L} + H_{\rm NL}, \tag{12}$$

where [19, 21, 39]

$$H_L = \sum_j \int \mathrm{d}\omega_j \hbar\omega_j a^\dagger_{j,\omega_j} a_{j,\omega_j}, \tag{13}$$

$$H_{\rm NL} = -\gamma_0 \int \mathrm{d}\omega_p \mathrm{d}\omega_s \mathrm{d}\omega_i a^\dagger_{p,\omega_p} a^\dagger_{p,\omega_p} a_{s,\omega_s} a_{i,\omega_i} e^{i(2k_p - k_s - k_i)x} + \mathrm{h.c.}, \tag{14}$$

where γ_0 denotes the effective coupling constant, $a^\dagger_m$ and a_m are the creation and annihilation operator of the degenerate FWM process represented by $\mu \in \{p, s, i\}$, $h.c.$ is the Hermitian conjugate.

The biphoton state generated from the FWM process is given by

$$|\Psi\rangle = \iint \mathrm{d}\omega_s \mathrm{d}\omega_i A(\omega_s,\omega_i) \hat{a}^\dagger_{\omega_s} \hat{a}^\dagger_{\omega_i} |0\rangle, \tag{15}$$

where $A(\omega_s,\omega_i)$ is the joint spectral amplitude. Consider the phase-matching condition and classical approximation of pump wave, it can be rewritten by

$$|\Psi\rangle = \iint \mathrm{d}\omega_s \mathrm{d}\omega_i \alpha \left(\frac{\omega_s + \omega_i}{2}\right) \mathrm{sinc}\left(\frac{\Delta k L}{2}\right) a_{s,\omega_s} a_{i,\omega_i} |0\rangle, \tag{16}$$

where Δk is the wavevector mismatch and L is the propagating length of topological kink states.

Appendix D. Robustness against disorders

To clarify the disorder stability of the FWM process in topological photonic crystals, we introduce disorders to the interface between trivial and nontrivial regions. As depicted in figure 6(b), inside the blue region, the positions of several rods are shifted randomly by the distances in the range of [−0.1a, 0.1a], and some selected rods are removed randomly. The simulated field profiles of the FWM process in photonic crystals are shown in figure 6(a). Topological edge states of the pump, signal, and idler are excited at a trapezoidal interface. We show that the biphoton states generated via the FWM process can pass through the disordered region without visible scattering. The field profiles of biphoton states are concentrated at the interface. The result implies that topological edge states of the pump, signal, and idler remain stable against these disorders. Such disorder stability comes from the lattice symmetry of the QSH effect. It is noted that the topological protection is destroyed when the C_6 symmetry of lattices is broken. In this case, the edge states are scattered into bulk bands.

ORCID iD

Guangqiang He https://orcid.org/0000-0001-9017-4159

References

[1] Haldane F and Raghu S 2008 Possible realization of directional optical waveguides in photonic crystals with broken time-reversal symmetry *Phys. Rev. Lett.* **100** 013904
[2] Raghu S and Haldane F D M 2008 Analogs of quantum-Hall-effect edge states in photonic crystals *Phys. Rev.* A **78** 033834
[3] Hafezi M, Mittal S, Fan J, Migdall A and Taylor J 2013 Imaging topological edge states in silicon photonics *Nat. Photon.* **7** 1001–5
[4] Slobozhanyuk A, Mousavi S H, Ni X, Smirnova D, Kivshar Y S and Khanikaev A B 2017 Three-dimensional all-dielectric photonic topological insulator *Nat. Photon.* **11** 130–6

[5] Cheng X, Jouvaud C, Ni X, Mousavi S H, Genack A Z and Khanikaev A B 2016 Robust reconfigurable electromagnetic pathways within a photonic topological insulator *Nat. Mater.* **15** 542–8

[6] Gao F, Xue H, Yang Z, Lai K, Yu Y, Lin X, Chong Y, Shvets G and Zhang B 2018 Topologically protected refraction of robust kink states in valley photonic crystals *Nat. Phys.* **14** 140–4

[7] Wu X, Meng Y, Tian J, Huang Y, Xiang H, Han D and Wen W 2017 Direct observation of valley-polarized topological edge states in designer surface plasmon crystals *Nat. Commun.* **8** 1304

[8] He X-T, Liang E-T, Yuan -J-J, Qiu H-Y, Chen X-D, Zhao F-L and Dong J W 2019 A silicon-on-insulator slab for topological valley transport *Nat. Commun.* **10** 872

[9] Peterson C W, Benalcazar W A, Hughes T L and Bahl G 2018 A quantized microwave quadrupole insulator with topologically protected corner states *Nature* **555** 346–50

[10] Mittal S, Orre V V, Zhu G, Gorlach M A, Poddubny A and Hafezi M 2019 Photonic quadrupole topological phases *Nat. Photon.* **13** 692–6

[11] Serra-Garcia M, Peri V, Süsstrunk R, Bilal O R, Larsen T, Villanueva L G and Huber S D 2018 Observation of a phononic quadrupole topological insulator *Nature* **555** 342–5

[12] Wu L-H and Hu X 2015 Scheme for achieving a topological photonic crystal by using dielectric material *Phys. Rev. Lett.* **114** 223901

[13] Smirnova D, Kruk S, Leykam D, Melik-Gaykazyan E, Choi D-Y and Kivshar Y 2019 Third-harmonic generation in photonic topological metasurfaces *Phys. Rev. Lett.* **123** 103901

[14] Kruk S S, Gao W, Choi D-Y, Zentgraf T, Zhang S and Kivshar Y 2021 Nonlinear imaging of nanoscale topological corner states *Nano Lett.* **21** 4592–7

[15] Kirsch M S, Zhang Y, Kremer M, Maczewsky L J, Ivanov S K, Kartashov Y V, Torner L, Bauer D, Szameit A and Heinrich M 2021 Nonlinear second-order photonic topological insulators *Nat. Phys.* **17** 995–1000

[16] Kruk S, Poddubny A, Smirnova D, Wang L, Slobozhanyuk A, Shorokhov A, Kravchenko I, Luther-Davies B and Kivshar Y 2019 Nonlinear light generation in topological nanostructures *Nat. Nanotechnol.* **14** 126–30

[17] You J W, Lan Z and Panoiu N C 2020 Four-wave mixing of topological edge plasmons in graphene metasurfaces *Sci. Adv.* **6** eaaz3910

[18] Barik S, Karasahin A, Flower C, Cai T, Miyake H, DeGottardi W, Hafezi M and Waks E 2018 A topological quantum optics interface *Science* **359** 666–8

[19] Mittal S, Goldschmidt E A and Hafezi M 2018 A topological source of quantum light *Nature* **561** 502–6

[20] Mittal S, Orre V V, Goldschmidt E A and Hafezi M 2021 Tunable quantum interference using a topological source of indistinguishable photon pairs *Nat. Photon.* **15** 542–8

[21] Blanco-Redondo A, Bell B, Oren D, Eggleton B J and Segev M 2018 Topological protection of biphoton states *Science* **362** 568–71

[22] Wang Y, Pang X-L, Lu Y-H, Gao J, Chang Y-J, Qiao L-F, Jiao Z-Q, Tang H and Jin X M 2019 Topological protection of two-photon quantum correlation on a photonic chip *Optica* **6** 955–60

[23] Chen C, Ding X, Qin J, He Y, Luo Y-H, Chen M-C, Liu C, Wang X-L, Zhang W-J and Li H 2018 Observation of topologically protected edge states in a photonic two-dimensional quantum walk *Phys. Rev. Lett.* **121** 100502

[24] Jiao Z-Q, Gao J, Zhou W-H, Wang X-W, Ren R-J, Xu X-Y, Qiao L-F, Wang Y and Jin X M 2021 Two-dimensional quantum walks of correlated photons *Optica* **8** 1129–35

[25] Chen Y, He X-T, Cheng Y-J, Qiu H-Y, Feng L-T, Zhang M, Dai D-X, Guo G-C, Dong J-W and Ren X F 2021 Topologically protected valley-dependent quantum photonic circuits *Phys. Rev. Lett.* **126** 230503

[26] Tambasco J-L, Corrielli G, Chapman R J, Crespi A, Zilberberg O, Osellame R and Peruzzo A 2018 Quantum interference of topological states of light *Sci. Adv.* **4** eaat3187

[27] Nie W, Peng Z, Nori F and Liu Y X 2020 Topologically protected quantum coherence in a superatom *Phys. Rev. Lett.* **124** 023603

[28] Jiang Z, Ding Y, Xi C, He G and Jiang C 2021 Topological protection of continuous frequency entangled biphoton states *Nanophotonics* **10** 4019–26

[29] Yang Y, Xu Y F, Xu T, Wang H-X, Jiang J-H, Hu X and Hang Z H 2018 Visualization of a unidirectional electromagnetic waveguide using topological photonic crystals made of dielectric materials *Phys. Rev. Lett.* **120** 217401

[30] He C, Ni X, Ge H, Sun X-C, Chen Y-B, Lu M-H, Liu X-P and Chen Y-F 2016 Acoustic topological insulator and robust one-way sound transport *Nat. Phys.* **12** 1124–9

[31] Yves S, Fleury R, Berthelot T, Fink M, Lemoult F and Lerosey G 2017 Crystalline metamaterials for topological properties at subwavelength scales *Nat. Commun.* **8** 16023

[32] Proctor M, Craster R V, Maier S A, Giannini V and Huidobro P A 2019 Exciting pseudospin-dependent edge states in plasmonic metasurfaces *ACS Photonics* **6** 2985–95

[33] Howell J C, Bennink R S, Bentley S J and Boyd R W 2004 Realization of the Einstein–Podolsky–Rosen paradox using momentum-and position-entangled photons from spontaneous parametric down conversion *Phys. Rev. Lett.* **92** 210403

[34] Mancini S, Giovannetti V, Vitali D and Tombesi P 2002 Entangling macroscopic oscillators exploiting radiation pressure *Phys. Rev. Lett.* **88** 120401

[35] Law C, Walmsley I A and Eberly J 2000 Continuous frequency entanglement: effective finite Hilbert space and entropy control *Phys. Rev. Lett.* **84** 5304

[36] MacLean J-P W, Donohue J M and Resch K J 2018 Direct characterization of ultrafast energy-time entangled photon pairs *Phys. Rev. Lett.* **120** 053601

[37] Wang L, Kruk S, Koshelev K, Kravchenko I, Luther-Davies B and Kivshar Y 2018 Nonlinear wavefront control with all-dielectric metasurfaces *Nano Lett.* **18** 3978–84

[38] König M, Wiedmann S, Brüne C, Roth A, Buhmann H, Molenkamp L W, Qi X-L and Zhang S C 2007 Quantum spin Hall insulator state in HgTe quantum wells *Science* **318** 766–70

[39] Silverstone J W, Bonneau D, Ohira K, Suzuki N, Yoshida H, Iizuka N, Ezaki M, Natarajan C M, Tanner M G and Hadfield R H 2014 On-chip quantum interference between silicon photon-pair sources *Nat. Photon.* **8** 104–8